Global bifurcations in a laser with injected signal: Beyond Adler's approximation

Martín G. Zimmermann[a)]
Departamento de Física, Facultad Ciencias Exactas y Naturales, Universidad de Buenos Aires, Ciudad Universitaria, 1428 Buenos Aires, Argentina

Mario A. Natiello
Center for Mathematical Sciences (LTH), Lund University, S-221 00 Lund, Sweden

Hernán G. Solari[b)]
Departamento de Física, Facultad Ciencias Exactas y Naturales, Universidad de Buenos Aires, Ciudad Universitaria, 1428 Buenos Aires, Argentina

(Received 22 January 2001; accepted 3 July 2001; published 28 August 2001)

We discuss the dynamics in the laser with an injected signal from a perturbative point of view showing how different aspects of the dynamics get their definitive character at different orders in the perturbation scheme. At the lowest order Adler's equation [Proc. IRE **34**, 351 (1946)] is recovered. More features emerge at first order including some bifurcations sets and the global reinjection conjectured in Physica D **109**, 293 (1997). The type of codimension-2 bifurcations present can only be resolved at second order. We show that of the two averaging approximations proposed [Opt. Commun. **111**, 173 (1994); Quantum Semiclassic. Opt. **9**, 797 (1997); Quantum Semiclassic. Opt. **8**, 805 (1996)] differing in the second order terms, only one is accurate to the order required, hence, solving the apparent contradiction among these results. We also show in numerical studies how a homoclinic orbit of the Šil'nikov type, bifurcates into a homoclinic tangency of a periodic orbit of vanishing amplitude. The local vector field at the transition point contains a Hopf-saddle-node singularity, which becomes degenerate and changes type. The overall global bifurcation is of codimension-3. The parameter governing this transition is θ, the cavity detuning (with respect to the atomic frequency) of the laser. [DOI: 10.1063/1.1397757]

The dynamics of a laser under the influence of an external signal is an important issue in laser applications, especially in the fields of communications and signal steering. This reason and the variety of nonlinear behavior that it can display have turned this laser into the subject of several studies. The locked–unlocked (to the external signal) transition can proceed in a simple form (for small injected signals) such as the one predicted by Adler's equation[1] or display period doubling cascades, Šil'nikov chaos, quasiperiodic solutions and more for larger values of injected signals. The organization of the dynamics can be understood by the concurrent effects of a Hopf-saddle-node (local) bifurcation coupled with a global reinjection mechanism. The back-bone of this organization was analytically unraveled using averaging (i.e., perturbative) techniques[2] which classified these systems in three qualitatively different regimes depending on the detuning of the host. The back-bone classification and the understanding achieved were partially challenged in Ref. 3 using a similar averaging technique. In the present work we review the different perturbation techniques orderwise, starting from Adler's equation. We find that the results in Ref. 2 have a larger range of applicability than those in Ref. 3 thus rendering a more accurate description of the laser than the one achieved in Ref. 4. We also provide a sound perturbative basis for the model advanced in Ref. 5. Furthermore we establish more accurate estimates of the critical detunings of the host where the transitions occur using normal-form analysis. The dynamics in the large detunings regime was studied previously in Ref. 5, where Šil'nikov chaos close to the locked–unlocked transition was revealed. The dynamics in the small detuning regime was described in Ref. 6, displaying a complicated sequence of secondary bifurcations as well. In the present study we analyze the transition to the intermediate detuning regime of the host laser. Instead of Šil'nikov chaos, a complex structure of homoclinic and heteroclinic connections associated to an unstable periodic orbit (known as undamped relaxation oscillation) is found. This new complex scenario is once more compatible with the Hopf-saddle-node local bifurcation coupled to a global reinjection of the type presented in Ref. 5.

I. INTRODUCTION

Early analysis of a laser with an injected signal (LIS)[7] revealed that the competition between different frequencies involved in the laser leads to a ''locking'' phenomenon. For very low injection amplitude and comparatively large frequency mismatch, the output frequency changes slightly with respect to the unperturbed laser, while for a (higher) critical

a)Electronic mail: zeta@df.uba.ar, http://www.nld.df.uba.ar
b)Electronic mail: solari@df.uba.ar

injection, locking to the external frequency occurs. The first model to capture this behavior was Adler's phase equation,[1] which in bifurcation terms exhibits a saddle-node infinite-periodic or Andronov bifurcation:[8] this is a well studied example of a local bifurcation (saddle-node) interacting with a global reinjection.

However, numerical experiments on the full 3-dimensional LIS rate equations produced a wealth of other phenomena (Hopf bifurcations,[9,10] period-doubling cascades,[7,11,12] quasiperiodicity[9,13]) which cannot be accounted for with just a phase variable. By the use of the averaging technique, a phase and amplitude reduced model was put forward,[2] which allowed a thorough analytical study of an extended portion of the rich bifurcation set of LIS.

Among the main features of LIS accounted for by the averaged equations there are the previous Andronov bifurcation, and the occurrence of undamped oscillations of the amplitude of the electric field (known as relaxation oscillations) which originate in a Hopf bifurcation. Solari and Oppo[2] also discussed the occurrence of a Hopf-saddle-node bifurcation (HSN), when the saddle-node and Hopf bifurcation become tangent in a two-parameter bifurcation set.[14,15] The unfolding of this local bifurcation presents four different cases (or types) depending on the sign of the nonlinear resonance terms.[14,15] Solari and Oppo established that the cavity detuning θ controlled which of the HSN types occurs in LIS as follows:

$$\begin{aligned} &\text{Type II:} \quad 0<\theta<\theta_{\text{II-I}};\\ &\text{Type I:} \quad \theta_{\text{II-I}}<\theta<\theta_{\text{I-III}};\\ &\text{Type III:} \quad \theta_{\text{I-III}}<\theta, \end{aligned} \tag{1}$$

with $\theta_{\text{II-I}}=1$ and $\theta_{\text{I-III}}=\sqrt{3}$ [where θ is a dimensionless quantity measuring the detuning of the cavity in terms of the characterized decay frequencies, see Eqs. (3)].

In view of the fact that there is a morphological identity between the equations for a gaseous laser where the polarization has been adiabatically eliminated[2,9] and those of a semiconductor laser,[3,4] the results of the present discussion apply to the latter laser, θ being interpreted as the line enhancement factor (usually named the α-factor).

However, a recent analysis[4] of the equations obtained after a similar averaging technique by Ref. 3 did not display the intermediate region $\theta_{\text{II-I}}<\theta<\theta_{\text{I-III}}$, in contradiction with the previous results in Ref. 2. One of the crucial differences between Types I and III of HSN is the location of the periodic orbit in parameter space. Figure 1 illustrates a schematic two-parameter bifurcation diagram for the normal form equation for HSN [see Eqs. (26)]. The saddle-node bifurcation set divides the HSN parameter plane in two connected regions; the Hopf bifurcation set lies within one of these regions (the upper region) being tangent to the saddle-node line at the HSN point. In Type III, the periodic orbit born in the Hopf bifurcation exists in the upper region, above the Hopf-line while in the Type I it exists in the lower region (all the way up to the Hopf-line) and it is of saddle type.

This difference is of decisive importance when a rigorous analysis of global bifurcations associated to either the fixed points or the periodic orbit in the HSN unfolding is

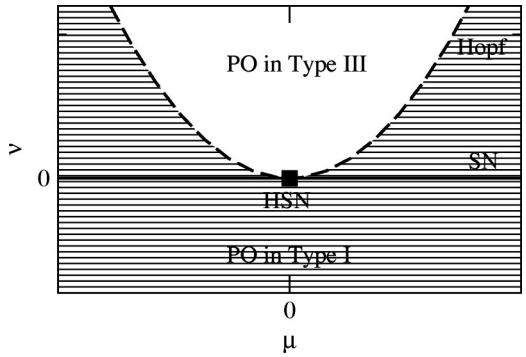

FIG. 1. Schematic two-parameter bifurcation diagram for the Hopf-saddle-node normal form, Eqs. (26). The locus of the saddle-node lies in $\nu=0$, while the locus of the Hopf bifurcation (dashed curve) lies on the parabola $\nu=\mu^2/a^2$. The HSN singularity lies at the tangent point of both sets. The Hopf bifurcation creates a periodic orbit in the parameter region $\nu>\mu^2/a^2$ for Type III (PO in Type III), while a saddle periodic orbit for Type III exists in the region $\nu<\mu^2/a^2$ (PO in Type I, dashed region).

studied. Global bifurcations for Type III were analyzed in Ref. 5, for the full 3-dimensional LIS equations. Numerically we studied the existence of Šil'nikov orbits to saddle-focus fixed points of HSN. Furthermore, one of these homoclinic bifurcations was found to become degenerate in a Šil'nikov-saddle-node bifurcation, where a homoclinic orbit to a saddle-node-focus fixed point occurs.[8,16] Analytically, we developed a geometric model to study the periodic orbit organization around this degenerate bifurcation, which conjectured a global reinjection mechanism as a basic ingredient for the global bifurcations in this type. A recent analysis of this laser system[6,17] corresponding to a cavity detuning in Type II, supports the results that the global reinjection present in LIS together with the HSN type are responsible for the organization of bifurcations. The global reinjection appears in the averaged equation as an invariant subspace.

Our goal in this manuscript is twofold. On one hand, present a consistent perturbation-approximation framework to the laser equations in order to consistently incorporate larger degrees of complexity in the model, going from the Adler equation at the lowest order to the averaged equations of Ref. 2 [with correct second order and errors of order $O(r^3)$] and giving a perturbative basis to the conjectured features of the geometric model of Ref. 5. We establish that LIS equations in fact have the three different types organized as in (1) and we obtain accurate values of the critical θ's where the transitions occur (we explain the differences with Ref. 3 in the Appendix).

On the other hand, we analyze the global bifurcations present in the 3-dimensional LIS equations as the type of HSN varies from Type III to Type I. We analyze this problem numerically and show how the Šil'nikov bifurcation to fixed points persists precisely up to the critical $\theta=\theta_{\text{I-III}}$, where a new higher codimension global bifurcation is found. In Type I ($\theta_{\text{II-I}}<\theta<\theta_{\text{I-III}}$), homoclinic bifurcations due to the global reinjection persists, but instead of involving the locking solutions it involves the saddle periodic orbit, which distinguishes Type I from Type III in the HSN. We analyze the global manifold organization and show that the homoclinic tangencies tend asymptotically to the HSN point in a two-

parameter unfolding of the bifurcation. Our result also implies that the resulting homoclinic tangle[14] is shown to exist in parameter regions having no locking solutions (as opposed to Type III, where chaos is observed coexisting with the locking region).

In the next section we introduce the LIS equations, we revisit the averaging procedure and derive its simplest invariant solutions. In Sec. III we derive the locus of the Hopf-saddle-node bifurcation for the 3-dimensional LIS equations and perform the normal form computations around this singularity. In Sec. IV we study numerically how the global bifurcations change when the local bifurcation changes from Type III to Type I. In Sec. V we discuss and sum up our results.

II. THE LASER EQUATIONS

The single-mode rate equations for a laser with an injected signal can be deduced from the Maxwell–Bloch equations, which consist of an equation for the slowly-varying complex electric field, one for the complex material polarization and finally an equation for the population inversion. Physically, the system presents a competition between different frequencies: the cavity eigenfrequency ω_c, the atomic eigenfrequency ω_a, and the external injection signal ω_{ext}. The electric field decays with a time constant proportional to $1/k$, the polarization with $1/\gamma_\perp$, and the population inversion with $1/\gamma_\parallel$. It has been shown that when $\gamma_\parallel \ll \gamma_\perp + k$, the polarization of the medium can be adiabatically eliminated.[2,9,18] This effectively reduces the laser equations to a 3-dimensional dynamical system in terms of $E(t)$, the complex electric field and $W(t)$, which is proportional to the population inversion. We will write the equations on a reference frame rotating with ω_{ext}:[3]

$$\begin{aligned} E' &= (1+i\theta)EW + i\eta E + \beta, \\ W' &= A^2 - \chi W(1+g|E|^2) - |E|^2, \end{aligned} \tag{2}$$

with the time t measured in units of $[(1+\theta^2)(\gamma_\perp + k)/k\gamma_\perp\gamma_\parallel]^{1/2}$. The three frequencies define two detunings:

$$\theta = \frac{\omega_c - \omega_a}{k+\gamma_\perp}, \qquad \eta = \omega_{\text{ext}} - \frac{k\omega_a + \gamma_\perp \omega_c}{k+\gamma_\perp}; \tag{3}$$

θ is proportional to the cavity detuning with respect to the atomic eigenfrequency, η is proportional to the detuning of the injected frequency with the unperturbed laser frequency, while

$$\chi = \left(\frac{\gamma_\parallel (1+\theta^2)(\gamma_\perp + k)}{k\gamma_\perp} \right)^{1/2} \tag{4}$$

is the decay rate of the population inversion measured in the new time units. The analysis of this paper covers a large literature of semiconductor laser dynamics, in which case the parameter θ in (2) is the linewidth enhancement factor. The parameter β corresponds to the rescaled amplitude of the injection, $g = \gamma_\perp/(k+\gamma_\perp)(1+\theta^2) \leqslant 1$ comes from the procedure to adiabatically eliminate the material polarization and A is the pumping with respect to the laser threshold.

We will consider β and η as bifurcation parameters (as well as θ when considering transitions between types in HSN), while χ is regarded as a small coefficient. Moreover, although many solid state lasers have g of order one, we will sometimes set $g=0$ since this simplification does not alter the qualitative bifurcation features. The pumping will always remain $A = \mathcal{O}(1)$. For the sake of perturbation theory our "small" parameters will be as it is in practice β and χ, corresponding to a small injected signal[19] on a low-dissipation laser device. All the numerical results presented in the figures, unless otherwise stated, are computed for $A=1$, $g=0$ and $\chi = 0.3$.

In polar coordinates $E(t) = R(t)e^{i\psi(t)}$, (2) reads as

$$\begin{aligned} R' &= RW + \beta\cos\psi, \\ W' &= A^2 - R^2 - \chi W(1+gR^2), \\ \psi' &= \eta + \theta W - \frac{\beta}{R}\sin\psi. \end{aligned} \tag{5}$$

Without perturbations ($\beta = \eta = \chi = 0$) the laser equations present reflection and rotation symmetries in the $W=0$ plane,[20] which account for an $O(2)$ symmetry in (5). This is reflected in the circle of fixed points having $(R,W,\psi) = (A,0,\psi)$, for arbitrary ψ. When the reflection symmetry is broken ($\eta \neq 0$), a periodic orbit appears, and exists for a range of β roughly up to the region where locking solutions appear.[5] Physically this solution corresponds to the *cw (continuous wave) solution* of the unperturbed laser, and has been studied with perturbation theory.[9]

Due to the competition of the various frequencies, this system presents locking behavior. For a given injection amplitude β, there is a detuning η such that the phase of the electric field locks to the injected source. This corresponds, in the rotating frame we are considering (2), to an equilibrium point. Actually, we find from the fixed point equations,

$$\begin{aligned} &\beta\cos\psi + RW = 0, \\ &A^2 - R^2 - \chi W(1+gR^2) = 0, \\ &-\beta\sin\psi + (\eta + \theta W)R = 0, \end{aligned} \tag{6}$$

a third order polynomial in R^2 (after having eliminated ψ and W) whose roots correspond to three possible fixed points. For the parameter values of interest (small β) it is found that two of them (corresponding to the locked solutions) arise in a saddle-node bifurcation, while the third, approximately at $(R,W) \simeq (0, A^2/\chi)$, corresponds to the "zero-intensity" equilibrium. Physically, this solution represents a laser radiating no electric field while the population inversion is saturated; it must be an unstable solution when the laser is on.

A. Consistent approximations

We start by considering solutions far away from $|E|/A \approx 0$, and perform the change of variables $v = \ln(R/A)$ on (5) to obtain

$$\begin{aligned} v' &= W + \frac{\beta}{A}e^{-v}\cos\psi, \\ W' &= A^2(1-e^{2v}) - \chi W(1+gA^2e^{2v}), \end{aligned} \tag{7}$$

$$\psi' = \eta + \theta W - \frac{\beta}{A} e^{-v} \sin\psi.$$

For $\beta = \chi = 0$ the variables (v, W) respond to a Hamiltonian dynamics[21] with Hamiltonian $H = W^2/2 + A^2(e^{2v}/2 - v)$, while the equation for ψ is decoupled.

We review the approximation scheme of Ref. 2, which consists of two parts: (i) the normal form theory to eliminate nonresonant terms for the unperturbed system, i.e., a change of variables to render the equations more manageable and (ii) averaging of the fast motion. The normal form calculation eliminates quadratic terms $O(v, W)^2$ which appear in a Taylor expansion of (7) in terms of v. The change of coordinates reads as

$$\begin{aligned} v &= V - \frac{V^2}{3} - \frac{2}{3}U^2, \\ W &= f(U + \tfrac{2}{3}UV), \\ \psi &= \phi + \theta v + \alpha, \end{aligned} \tag{8}$$

with $f = \sqrt{2}A$ and $\alpha = \arctan(1/\theta)$ (we will hence use θ and α alternatively in order to display the simplest equations). The transformed system (7) becomes then, for small U, V, $\kappa = \beta/A$ and χ:

$$\begin{aligned} V' &= fU + \kappa\cos(\phi+\alpha) - \kappa V(\theta\sin(\phi+\alpha) \\ &\quad + \cos(\phi+\alpha)/3) + g_{v1}\chi U^2 + g_{v2}\kappa U^2 \\ &\quad + g_{v3}\kappa V^2 + O(\kappa,\chi,U,V)^4, \\ U' &= -fV - \chi(1+A^2g)U - \tfrac{2}{3}\kappa U\cos(\phi+\alpha) \\ &\quad + \tfrac{4}{3}fU^2V + g_{u1}\chi UV + g_{u2}\kappa UV + O(\kappa,\chi,U,V)^4, \end{aligned} \tag{9}$$

$$\begin{aligned} \phi' &= \eta - \kappa\frac{\cos(\phi)}{\sin\alpha} + \kappa(1+\theta^2)V\sin(\phi+\alpha) \\ &\quad + g_{\phi 1}\kappa U^2 + g_{\phi 2}\kappa V^2 + O(\kappa,\chi,U,V)^4, \end{aligned}$$

where the explicit coefficients for the cubic terms are

$$\begin{aligned} g_{v1} &= -\tfrac{4}{3}(1+A^2g), \quad g_{v2} = -\tfrac{2}{9}\cos(\phi+\alpha), \\ g_{v3} &= \left(\frac{11}{18} - \frac{\theta^2}{2}\right)\cos(\phi+\alpha) + \frac{2}{3}\theta\sin(\phi+\alpha), \\ g_{u1} &= -2A^2g, \quad g_{u2} = \frac{2\sin(\phi+2\alpha)}{3\sin\alpha}, \\ g_{\phi 1} &= -\frac{\cos\phi}{3} + \frac{\cos(\phi+2\alpha)}{3\sin^3\alpha}, \\ g_{\phi 2} &= -\frac{\cos\phi}{6} + 4\frac{\cos(\phi+2\alpha)}{\sin^3\alpha}. \end{aligned}$$

Notice that for no perturbations ($\kappa = \chi = 0$), and *truncating at order* $O(U,V)^3$, the system (9) decouples in a harmonic oscillator $V'' + f^2V = 0$ and a trivial phase $\phi(t) = \eta t$. The change of coordinates (8) effectively eliminates all quadratic terms of the form U^iV^{2-i}, $i = 0,1,2$ leaving a simple analytic solution from which to perturb. The lowest resonant terms are cubic, U^iV^{3-i}, $i = 0,\ldots,3$ *even* when $\kappa = \chi = 0$ (term U^2V in U') and do not vanish for general values of the parameters. Indeed, in the variables (U,V), we have the Hopf normal form structure.[14] The oscillation (labeled RO) which arises in the (U,V) plane is physically interpreted as a relaxation oscillation.

The next step in the procedure involves recasting (9) in the standard "slow" vector field form required for averaging:[14] $x' = \epsilon F(x,t;\epsilon)$, where $0 < \epsilon \ll 1$ and F is T-periodic in t. We therefore make a new change of coordinates which rotates with the unperturbed ($\kappa = \chi = 0$) harmonic solution: $V(t) = r(t)\cos(ft - \xi(t)), U(t) = -r(t)\sin(ft - \xi(t))$, where (r,ξ) are the new variables. In the frame of reference of the RO, the resulting dynamics is effectively "slow" and we can average those time dependent terms in the equation over one period of the RO. We arrive at the averaged equations:

$$\begin{aligned} r' &= -\frac{r}{2}\left((1+A^2g)\chi + \kappa\frac{\sin(\phi+2\alpha)}{\sin(\alpha)}\right), \\ \phi' &= \eta - \kappa\frac{\cos(\phi)}{\sin\alpha} - \kappa\frac{r^2}{4\sin^3\alpha}(\cos\phi - 2\cos(\phi+2\alpha)), \end{aligned} \tag{10}$$

with $\xi' = 0$, *with errors of order* $O(r^3, \kappa^2, \chi^2)$.

Another set of averaged equations has been derived in Ref. 3. Their resulting system departs from (10) in the quadratic terms, thus being insufficient to describe the original equations beyond first order. For an analysis of the validity limits of the results in Ref. 3 see Appendix A, where we recover the averaged system analyzed in Ref. 4. Since the second-order terms are crucial to describe the bifurcation scenario of LIS (see below), the model in Ref. 3 will not display the features of the system in a proper way. Indeed, the (otherwise thorough) analysis in Ref. 4 does not present the Type I behavior and expects a transition from Type II to Type III of HSN at $\theta = 1$. We will establish below (see Sec. III B) using normal form theory that the classification (1) is the correct description of the HSN bifurcation.

B. Adler's model and beyond

Let us perform an order-by-order analysis of Eqs. (9) and (10). Retaining only first order terms in the expansion parameters κ, χ, U and V and performing then the averaging we obtain a decoupled system consisting of an oscillator plus a phase equation, i.e., an Adler equation:

$$\phi' = \eta - \kappa\frac{\cos\phi}{\sin\alpha}. \tag{11}$$

The system displays a saddle-node bifurcation at the fixed point ($r = \text{const}, \phi = \pi$) for

$$\kappa_{SN} = \pm\,\eta\sin\alpha. \tag{12}$$

This equation signals locking behavior for a sufficiently large injection rate $\kappa \geqslant \kappa_{SN}$.

The next step in the perturbation approach could be to include second-order terms proportional to χ (assuming hence $\kappa \ll \chi$), which represents a situation where the dissipation of the laser overwins the injection rate of energy. We approximate then the equation for r' in (10) as $r' \approx -[(1+A^2g)/2]\chi r$ and notice that in this regime, the dynamics on

r asymptotically goes to $r=0$ after a short transient, and the Adler equation describes the motion in this submanifold.

Also, due to the invariant subspace $r=0$ of (10) a global bifurcation occurs at the critical parameter value. This bifurcation scenario is known as Andronov or saddle-node infinite-period bifurcation,[8] and involves the disappearance at $\kappa=\kappa_{SN}$ of the periodic orbit existing at $r=0$ for $\kappa<\kappa_{SN}$.

For injection rates of the order of $\kappa=O(\chi)$ we must consider the full equation for r' in (10). Finally, the next step in the approximation procedure is to include the terms up to second order in U and V and first order in κ and χ in (9), thus recovering the full equations (10). Normal form analysis[14] reveals that these terms are necessary to unfold the most important bifurcations. We will stop the perturbative expansion at this point, noting in passing that a more detailed analysis beyond the results in this and the coming sections demands the inclusion of terms of order three in U and V.

We may now refine the validation boundary of the Adler equation considering where the coupling between ϕ and r becomes important in (10). Indeed, a fixed point with $r>0$ in (10), corresponding to a *transversal* periodic orbit of the whole system, exists for $\phi=\phi_H$ such that $r'=0$, i.e., $\phi_H=-2\alpha-\arcsin((1+A^2g)\chi\sin(\alpha)/\kappa)$. Solving for the radius of the periodic orbit r_H^2 from ϕ' we arrive at

$$r_H^2(\eta,\kappa)=\left(\frac{4\sin^2\alpha}{\kappa}\right)\left(\frac{\eta\sin\alpha-\kappa\cos\phi_H}{\cos\phi_H-2\cos(\phi_H+2\alpha)}\right), \quad (13)$$

which shows the existence of a periodic orbit whenever $r_H>0$. The condition for a Hopf bifurcation becomes $r_H=0$ and is realized whenever

$$\kappa_H=\frac{\sin\alpha}{\cos 2\alpha}(\eta^2+2\eta\chi\sin 2\alpha+(1+A^2g)^2\chi^2)^{1/2}. \quad (14)$$

The Adler equation can be regarded to hold whenever $\kappa<\inf_\eta\kappa_H(\eta,\chi)=\chi(1+g)^2-(\sin 2\alpha)^2$.

The Hopf and saddle-node local bifurcations considered above are not independent. The bifurcation sets become tangent at

$$\kappa_{HSN}=\frac{\sin\alpha}{\sin 2\alpha}(1+A^2g)\chi,$$
$$\eta_{HSN}=-\frac{(1+A^2g)}{\sin 2\alpha}\chi, \quad (15)$$

which defines the location of the Hopf-saddle-node singularity in Eqs. (10).

C. Averaging and reinjection

Solari and Oppo[2] gave a comprehensive view of the bifurcations of Eqs. (10) organized around the HSN bifurcation for a large range of parameters. They extended the behavior observed in the simpler Adler's phase equation, still permitting analytical tractability of local bifurcations.

Nevertheless, some features of the averaged model involving global connections are nongeneric in $d>1$ dimensions, and deserve close attention. As noted in Ref. 14, the average procedure may obscure some things when it concerns global bifurcations. For example, the saddle-node infinite-period global bifurcation appearing at $r=0$ for $\kappa=\kappa_{SN}$ is a feature not expected to occur in the full 3-dimensional LIS equations.[22] This fact may be traced back to Eqs. (9), where the only term breaking the $r=0$ invariance is $\kappa\cos(\phi+\alpha)$ in the equation for V', which vanishes in the averaging procedure (after changing coordinates to the "slow" variables (r,ξ), it is multiplied by a trigonometric function of ft with zero average). Therefore, we may expect that higher order corrections to the averaging model will break this particular invariant submanifold.

In this direction, we have conjectured[5] that a geometric model of the full LIS equations with the following three ingredients should display the homoclinic and heteroclinic features numerically observed on the full LIS equations:

(1) A Hopf-saddle-node local dynamics.
(2) A global reinjection resembling the periodic orbit at $r=0$.
(3) A reinjection parameter destroying the $r=0$ invariance in the local normal form.

We will address the existence of a Hopf-saddle-node point in the full LIS equations (advanced in Ref. 6) in the next section. The existence of the periodic orbit has been sufficiently discussed above, and its effect on the reinjection will be clear from the equations below. We address now the remaining feature, which can be understood by perturbation analysis in (9) already at first order.

Let us reconsider Eqs. (9) truncated to first order at the parameter values for one of the saddle-node singularities $\eta=-\kappa/\sin\alpha=-\kappa\sqrt{1+\theta^2}$:

$$V'=fU+\frac{\eta}{1+\theta^2}(\theta\cos(\phi)-\sin(\phi)),$$
$$U'=-fV, \quad (16)$$
$$\phi'=-\eta(1+\cos(\phi)).$$

With this parameter choice the fixed point located at $V=0$, $U=\eta\theta/(f(1+\theta^2))$, $\phi=\pi$ destroys the periodic orbit signaling the occurrence of the saddle-node bifurcation. The LIS reinjection is here represented by the decoupled equation in ϕ: Initial conditions for $t\to-\infty$ near the fixed point at $\phi=\pi$ return to it (in the form $\phi=-\pi$) for $t\to+\infty$. The equation integrates to $\phi(t)=2\arctan(\eta t)$. We can now solve for V and U with suitable initial conditions near the fixed point. We let $z=V+iU$ and obtain $\dot z+ifz=[\eta/(1+\theta^2)]\times(\theta\cos(\phi)-\sin(\phi))$ which integrates to $z(t)=Be^{-ift}+p(t)$ where B is determined by the initial condition, which we take such that for very large positive X, $z(-X)=i\eta\theta/(f(1+\theta^2))$. Hence,

$$p(t)=\frac{\eta}{1+\theta^2}\int_{-X}^{t}e^{-if(t-s)}\frac{(1-\eta^2s^2)\theta+2\eta s}{1+\eta^2s^2}ds$$
$$=\frac{i\eta\theta}{f(1+\theta^2)}(1-e^{-if(t+X)})$$
$$+\frac{2\eta e^{-ift}}{f(1+\theta^2)}\int_{-X}^{t}e^{ifs}\frac{\theta+\eta s}{1+\eta^2s^2}ds,$$

and $B=i\eta\theta e^{-ifX}/(f(1+\theta^2))$. Approximating the remaining integral in $p(t)$ by an infinite integral via letting $t,X\to\infty$ we obtain

$$z(t)=\frac{i\eta\theta}{f(1+\theta^2)}+\frac{2\pi(i+\theta)}{1+\theta^2}e^{-f/\eta}e^{-ift}, \tag{17}$$

which represents a circle centered on the fixed point with radius

$$\overline{x}=\frac{2\pi e^{-f/\eta}}{\sqrt{1+\theta^2}}.$$

Hence, initial conditions close to $r=0$ are reinjected near the fixed point with a value around $r=\overline{x}$, as conjectured in Ref. 5. As expected, the averaging wipes out this effect, which is important when global bifurcations associated to the HSN fixed point/periodic orbit occurs.

III. DERIVATION OF THE CODIMENSION-2 SINGULARITY

We now turn to a detailed normal form analysis of the Hopf-saddle-node (HSN) bifurcation in the full 3-dimensional LIS equations. First we obtain the locus of this singularity in parameter space, and next we turn into the computation of the normal form coefficients, from which we may establish the critical cavity detunings θ where the type of HSN changes.

A. Hopf-saddle-node bifurcation

The Hopf-saddle-node bifurcation arises generally in vector fields whose Jacobian at the fixed point $\mathbf{x_0}=(\overline{R},\overline{W},\overline{\psi})$ has a pair of purely imaginary eigenvalues together with a zero eigenvalue: $\{0,\pm i\omega\}$ with $\omega>0$.[14,15]

The Jacobian of (5) at $\mathbf{x_0}$ is

$$\mathbf{J}=\begin{pmatrix} \overline{W} & \overline{R} & -\beta\sin\overline{\psi} \\ -2\overline{R}(1+g\chi\overline{W}) & -\chi(1+g\overline{R}^2) & 0 \\ \beta\sin\overline{\psi}/\overline{R}^2 & \theta & -\beta\cos\overline{\psi}/\overline{R} \end{pmatrix}, \tag{18}$$

and from the fixed point equations (6) we find

$$\begin{aligned} \overline{R}(\overline{W})&=\sqrt{\frac{A^2-\chi\overline{W}}{1+g\chi\overline{W}}}, \\ \overline{\psi}(\overline{W})&=-\arctan\left(\frac{\eta+\theta\overline{W}}{\overline{W}}\right), \end{aligned} \tag{19}$$

in terms of $\overline{W}$, leaving the characteristic polynomial of $\mathbf{J}$ in terms of $(\overline{W},\eta,\theta)$,

$$c_0+c_1\lambda+\left(\frac{1+gA^2}{1+g\chi\overline{W}}-2\overline{W}\right)\lambda^2+\lambda^3=0. \tag{20}$$

As the roots of the characteristic polynomial at the HSN bifurcation are $\{0,\pm i\omega\}$, the polynomial should read as $\lambda(\lambda^2+\omega^2)=0$. Equating the same order coefficients we arrive at

$$\begin{aligned} \overline{W}&=\frac{\chi(1+gA^2)}{2}+\mathcal{O}(\chi^3), \\ \omega^2&=c_1(\overline{W},\eta,\theta)>0, \\ 0&=c_0(\overline{W},\eta,\theta), \end{aligned} \tag{21}$$

having expanded the solution of $\overline{W}$ in terms of small χ. Note that for fixed g, χ, A and θ the system (21) can be exactly solved for the location of the fixed point and the parameter values $(\eta_{\mathrm{HSN}},\beta_{\mathrm{HSN}})$, as illustrated in Ref. 6. Using the above expression for $\overline{W}$ we can solve the last equation in (21) for $\eta(\theta)$. Using the fixed point equations (6), we have $\beta=-\overline{R}\,\overline{W}/\cos\overline{\psi}$ and together with (19) and the first equation in (21) we obtain the locus of the HSN at

$$\eta_{\mathrm{HSN}}(\theta)=-\frac{(1+\theta^2)}{2\theta}(1+gA^2)\chi+\mathcal{O}(\chi^3), \tag{22}$$

$$\beta_{\mathrm{HSN}}(\theta)=\frac{A\sqrt{1+\theta^2}}{2\theta}(1+gA^2)\chi+\mathcal{O}(\chi^3), \tag{23}$$

with

$$\omega_{\mathrm{HSN}}(\theta)=\sqrt{2}A+\frac{\chi^2}{8\sqrt{2}A}\left(7+10gA^2+3g^2A^4-\frac{(1+gA^2)^2}{\theta^2}\right)+\mathcal{O}(\chi^3), \tag{24}$$

in agreement with (15).

Performing the exact computations without the expansion in χ, we obtain for $\theta=2.0, g=0.0, \chi=0.3, A=1.0$, the numeric result:

$$(\eta_{\mathrm{HSN}},\beta_{\mathrm{HSN}})=(-0.372816,...,0.162945,...), \tag{25}$$

which compare very well with the approximate values using (23).

We conclude that the HSN singularity is intrinsic to the full LIS equations and not just a property of the averaged model. Also note that for $\chi\to 0$, the codimension-2 point approaches $(\eta,\beta)_{\mathrm{HSN}}=(0,0)$.

B. Derivation of the normal form coefficients

The normal form of HSN up to second order in cylindrical coordinates is[14]

$$\begin{aligned} r'&=(\mu+az)r+\mathcal{O}(3), \\ z'&=\nu+br^2+cz^2+\mathcal{O}(3), \\ \zeta'&=\omega+dz+\mathcal{O}(2), \end{aligned} \tag{26}$$

where $a,b,c\neq 0$ and μ and ν are the bifurcation parameters. Moreover, we can let $c=-1$ by rescaling (this is the traditional form).

The signs of a and b classify the different types of flows: Type I for $(a>0,b>0)$, Type II for $(a<0,b>0)$, Type III for $(a>0,b<0)$, Type IV for $(a<0,b<0)$. For $\nu_{\mathrm{sn}}=0$ one has a saddle-node bifurcation, while for $\nu_{\mathrm{Hopf}}=\mu^2/a^2$, the Hopf bifurcation occurs. The radius of the periodic orbit is given by $r^2_{\mathrm{Hopf}}=(\mu^2/a^2-\nu)/b$. Hence, the difference between the phase portraits in Type III and Type I is that in the

former, the periodic orbit always co-exists with the fixed points ($\nu > \mu^2/a^2 > 0$), while in the latter it may exist even before the creation of the fixed points (for $\nu < 0$, $r_{\mathrm{Hopf}} > 0$); see Fig. 1. The stability of the periodic orbit for Type I can be shown to be saddle, while for Type III may be an unstable or stable node. The above properties will be reflected in the global bifurcations found for either Type (see the next section).

Numerical experiments in Ref. 5 suggested that LIS equations have a Type III singularity for $\theta = 2.0$. The question we address now is what happens for other choices of θ and particularly if the classification found in Ref. 18 holds for the three-dimensional LIS equations (1). We will now derive approximate equations for $a(\theta)$, $b(\theta)$, $c(\theta)$, $d(\theta)$ assuming, once again, small χ.

We start by linearizing LIS equations (5) around the fixed point $\mathbf{x_0} = (\overline{R}, \overline{W}, \overline{\psi})$ at the HSN bifurcation parameter $(\eta_{\mathrm{HSN}}, \beta_{\mathrm{HSN}}, \theta)$. This may be accomplished by choosing a linear change of coordinates $\xi = \mathbf{U}^{-1}(\mathbf{x} - \mathbf{x_0})$, where $\mathbf{U}$ is the matrix having as first and second columns the real and imaginary part of the eigenvector of $\mathbf{J}$ associated to the eigenvalue $i\omega$ while the third column is the eigenvector associated to the zero eigenvalue. We find the matrix $\mathbf{U}$ reads [up to normalization constants, and showing up to $O(\chi)$ terms for the sake of clarity] as

$$\mathbf{U} \simeq \begin{pmatrix} A\theta & \frac{\sqrt{2}\chi}{4\theta}(1+\theta^2)(1+gA^2) & 0 \\ \frac{\chi}{2\theta}(1-\theta^2)(1+gA^2) & -\sqrt{2}A\theta & -\frac{\chi}{2\theta}(1+gA^2) \\ \theta^2 & 0 & 1 \end{pmatrix}, \tag{27}$$

and the new system $\xi = (x, y, v)$ reads as

$$\begin{aligned} x' &= -\omega y + F(x,y,v), \\ y' &= \omega x + G(x,y,v), \\ v' &= H(x,y,v), \end{aligned} \tag{28}$$

where $F(x,y,v)$, $G(x,y,v)$ and $H(x,y,v)$ carry only nonlinear terms.

The nonlinear coefficients of (26) can now be obtained in terms of derivatives of F, G and H (see Appendix B for the derivation). Up to first order in χ, we obtain

$$\begin{aligned} a(\theta) &= (F_{xv} + G_{yv})/2 = \frac{(\theta^2 - 1)}{4\theta}(1+gA^2)\chi + O(\chi^2), \\ b(\theta) &= (H_{xx} + H_{yy})/4 \\ &= -\frac{(1+\theta^2)(\theta^2 - 3)}{8\theta}(1+gA^2)\chi + O(\chi^2), \\ c(\theta) &= H_{vv}/2 = -\frac{(1+\theta^2)}{4\theta}(1+gA^2)\chi + O(\chi^2), \\ d(\theta) &= (G_{xv} - F_{yv})/2 = O(\chi^2). \end{aligned} \tag{29}$$

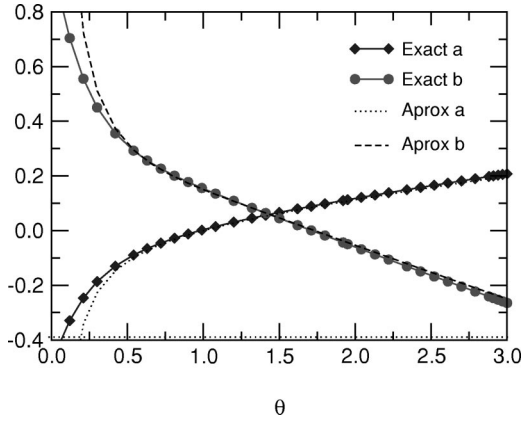

FIG. 2. Normal form coefficients $a(\theta)$ and $b(\theta)$ as a function of θ ($g = 0$, $\chi = 0.3$, $A = 1$).

We observe from (29) that $a(\theta)$ changes sign at $\theta_{\mathrm{II\text{-}I}} = 1 + \mathcal{O}(\chi^2)$ while $b(\theta)$ at $\theta_{\mathrm{I\text{-}III}} = \sqrt{3} + \mathcal{O}(\chi^2)$. In conclusion, the *Hopf-saddle-node singularity in the 3-dimensional LIS equations change their type according to the Solari and Oppo results* (1), up to order $\mathcal{O}(\chi^2)$.

The whole procedure to obtain the linear and nonlinear coefficients of the normal form may be evaluated numerically without using the expansions in χ. In Fig. 2 we compared the numerical evaluation with the approximate formulas given in (29). We find for $\chi = 0.3, g = 0$ that the critical cavity detunings become

$$\theta_{\mathrm{I\text{-}III}} = 1.71372..., \quad \theta_{\mathrm{II\text{-}I}} = 0.977794... . \tag{30}$$

Note that for small enough θ, the exact and the numeric approximation depart, due to the failure of the condition $\omega_{\mathrm{HSN}} > 0$ in (24) for evaluating the HSN coordinates.

IV. GLOBAL BIFURCATIONS

Simple numerical experiments on LIS equations [Eqs. (5)] starting from the *cw* solution in $\beta = 0$, $R = A$, $\psi = \eta t$, give us a qualitative picture of the dynamics in this laser. In Fig. 3 we display for two parameter cuts in η, phase portraits of this longitudinal orbit (on the $W = 0$ plane) as the injection level β is increased. It can be observed that part of the trajectory develops small oscillations in the transversal (to the

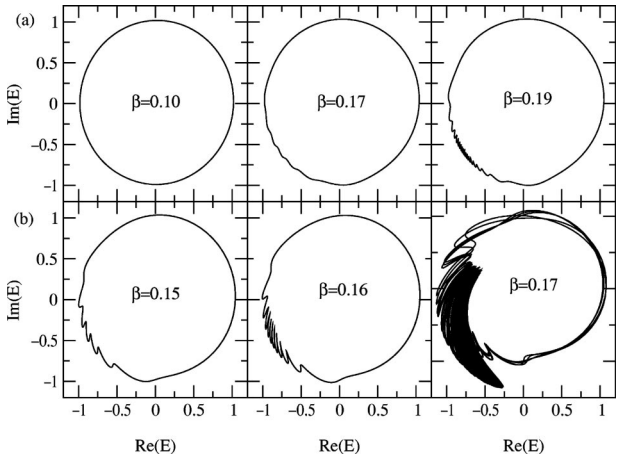

FIG. 3. Phase portraits of longitudinal attractors in LIS for increasing β. (a) Type I: $\theta=1.25$, $\eta=-0.3175$, (b) Type III: $\theta=2.0$, $\eta=-0.38$. The bottom right corresponds past the saddle-node bifurcation and is a strange attractor orbit.

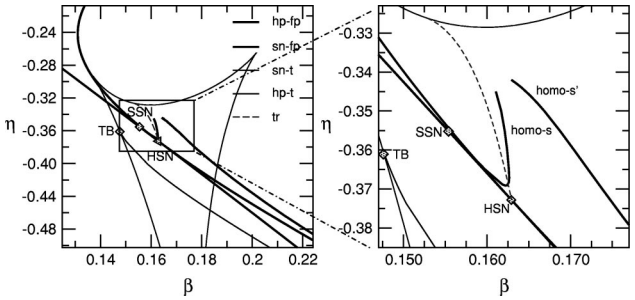

FIG. 5. A β vs η partial bifurcation set close to HSN for $\theta=2.0$ (Type III). The saddle-node (sn-fp) and the Hopf (hp-pf) bifurcation become tangent at the Hopf-saddle-node (HSN) bifurcation. In Type III a secondary Hopf bifurcation (tr) leading to a transversal torus and a global heteroclinic bifurcation between the two fixed points (not shown) originates from HSN. SSN denotes the Šil'nikov-saddle-node degenerate bifurcation point. TB denotes a Takens–Bogdanov degenerate point, where a Hopf (hp-t), a saddle-node (sn-t) and a homoclinic bifurcation (not shown), all collide at the same point.

$W=0$ plane) direction, and approximately on the phase position where the fixed points will be born ($R\approx A$, $\phi=\pi$) in a saddle-node bifurcation at $\beta=\beta_{\mathrm{SN}}$. One also observes that for higher θ (stronger phase coupling), the size of these oscillations is also larger. Below we will see that this orbit in fact leads to a family of similar orbits, in the neighborhood of $\beta\approx\beta_{\mathrm{SN}}$, with more and more transversal oscillations in that same region of phase space.

We call γ the transversal periodic orbit born at the Hopf bifurcation of fixed points. The properties of this orbit are in accordance with the results of the unfolding of HSN (Sec. III B) which depends strongly on the type of HSN.[14] For Type III the periodic orbit γ exists for $\beta\geqslant\beta_{\mathrm{Hopf}}>\beta_{\mathrm{SN}}$ and may be stable or unstable, both situations connected by a secondary Hopf bifurcation (labeled tr in Fig. 5). On the other hand, for Type I γ is a saddle orbit and exists for $\beta\leqslant\beta_{\mathrm{Hopf}}$, and may even exist before the locking solutions appear ($\beta<\beta_{\mathrm{SN}}$) as illustrated in Fig. 4. With the aid of AUTO94[23] the periodic orbit γ was found to belong to a family of transversal periodic orbits bounded in the relevant parameter space by a set of saddle-node bifurcations labeled sn-t in Fig. 5 and Fig. 6. The saddle-node companion of γ is shown with a full curve in Fig. 4. Associated to this family of transversal periodic orbits a Takens–Bogdanov singularity[14] was found, which guides another secondary Hopf bifurcation to the transversal orbit (labeled hp-t) and another homoclinic bifurcation (not shown in the bifurcation set).[24]

A. Extremely large detunings

In a previous study,[5] we studied global bifurcations for a fixed $\theta=2.0$, which correspond to the Type III regime of HSN. The main bifurcations were two Šil'nikov homoclinic orbits to either saddle-focus fixed points **S** or **S'** of the saddle-node bifurcation. The interesting phenomenon was that the branch of homoclinic orbit to **S** approached on one side asymptotically to the saddle-node bifurcation (the SSN point in Fig. 5). At the limit point there was a *degenerate* homoclinic orbit[25] to a saddle-node fixed point. The orbit left the vicinity of the degenerate equilibrium through the 1-dimensional center manifold and returned through the 2-dimensional stable manifold. This interaction has been called a Šil'nikov-saddle-node and requires 2-parameters (codimension-2) to unfold it.

We extend these results now and study the behavior of this degenerate bifurcation, as θ is decreased, in particular, as it approaches the critical $\theta=\theta_{\mathrm{I\text{-}III}}$ parameter value. To perform the numeric continuation of the Šil'nikov-saddle-node

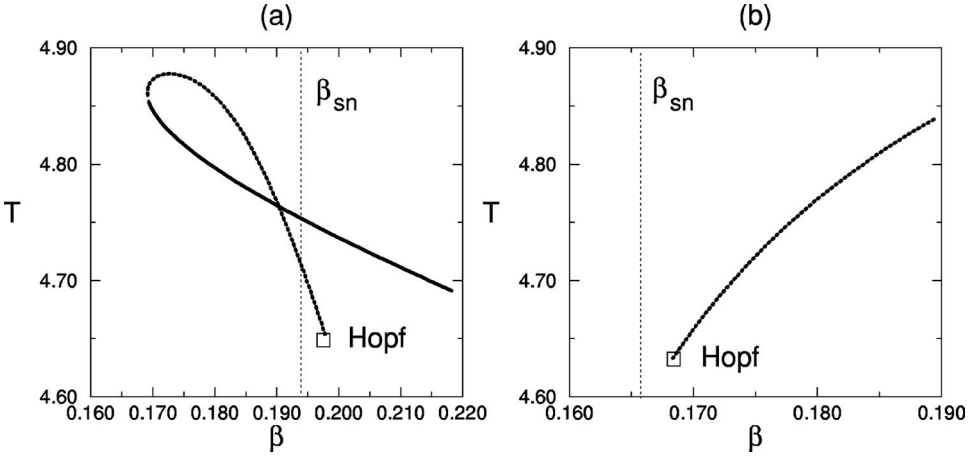

FIG. 4. Period T vs β of periodic orbit γ born at the Hopf bifurcation. (a) For Type I ($\theta=1.25$, $\eta=-0.3184$) the Hopf bifurcation creates a saddle periodic orbit γ which may exist before the creation of fixed points ($\beta<\beta_{\mathrm{SN}}$). Dashed strokes for γ and full stroke for its saddle-node companion. (b) For Type III ($\theta=2.0$, $\eta=-0.385$) γ is either a stable or an unstable node, coexisting with the fixed points. The vertical dashed line corresponds to the occurrence of the saddle-node bifurcation of the fixed points β_{SN}.

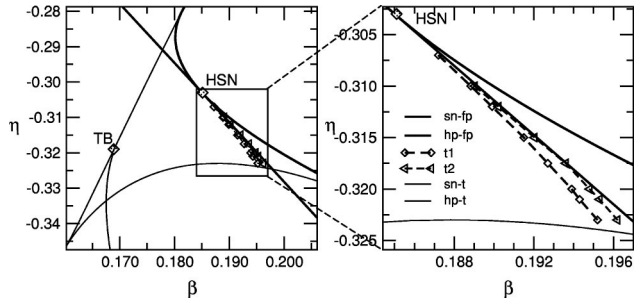

FIG. 6. A β vs η partial bifurcation set close to HSN for $\theta=1.25$. See Fig. 9 for a schematic bifurcation diagram. $(t1)$ corresponds to the homoclinic tangency to the periodic orbit γ, and similarly for $(t2)$. Also a Takens–Bogdanov point is found as in Fig. 5.

(SSN) point, we implemented a simple shooting algorithm. Choosing the parameters at the saddle-node bifurcation $\beta_{\mathrm{SN}}(\eta)$ we took an initial condition on the center manifold at a small distance of the singularity and integrated forward in time to a Poincaré section away from the saddle-node equilibrium. We then shot from a point ζ on the local 2-dimensional stable manifold backwards in time to that same Poincaré section, and chose the point ζ such that it minimized the distance of both intersections on the section. Next we changed η in order to assure that $z=0$. At this point in parameter space we have an approximate orbit which follows the degenerate Shinikov-saddle-node orbit.

In Table I we show the results of the continuation of the SSN point as a function of θ, together with the corresponding $b(\theta)$ coefficient of the normal form (26). It is observed that the SSN degeneracy approaches the HSN singularity at the detuning θ corresponding to the transition from Type III to Type I: $\theta_{\mathrm{I\text{-}III}}=1.71372$ (last row). This is the reason for performing an accurate determination of the location of the critical θ values in order to understand this limit behavior.

These results suggest that a *global codimension-3* bifurcation occurs for this laser model at $\theta_{\mathrm{I\text{-}III}}$. We are not aware of any theoretical result on the unfolding of such a degenerate bifurcation, so our numerical findings can serve as a ''suggested'' unfolding. Figure 7 displays the SSN homoclinic orbit very close to the transition point. We note that as we approach the critical detuning θ, the total integration time of the shooting implementation diverges, because the stable 2-dimensional manifold becomes a very slow manifold.

TABLE I. Continuation of the Šil'nikov-saddle-node point as $\theta\rightarrow\theta_{\mathrm{I\text{-}III}}$.

θ	η_{SSN}	β_{SSN}	$b(\theta)$
2.00	−0.355212	0.155423	−0.0601082
1.90	−0.349017	0.158996	−0.0391471
1.80	−0.343095	0.162927	−0.0181445
1.75	−0.340707	0.165260	−0.0076315
1.74	−0.340420	0.165827	−0.0055281
1.72	−0.340582	0.167325	−0.0013205
1.71372	−0.341865...	0.168392...	0.0

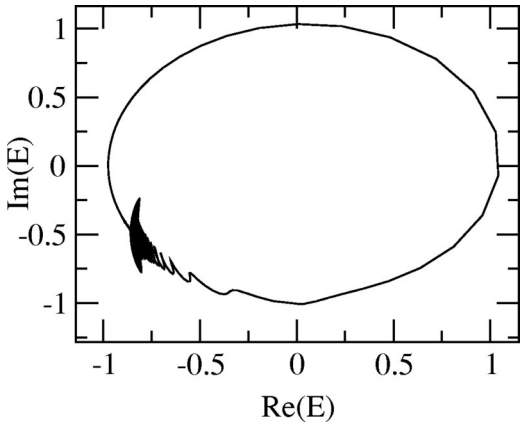

FIG. 7. A Šil'nikov orbit close to Hopf-saddle-node bifurcation at $\theta=1.72$, $\eta_{\mathrm{SSN}}=-0.3405825055$, $\beta_{\mathrm{SSN}}=0.1673253154$. The change of type occurs at $\theta_{\mathrm{I\text{-}III}}=1.71372...$, $\eta=-0.341866...$, $\beta=0.168393...$.

B. Large detunings

We now describe the global bifurcations for $\theta_{\mathrm{II\text{-}I}}<\theta<\theta_{\mathrm{I\text{-}III}}$ corresponding to the Type I regime. Note that from the local phase portraits for the HSN (see Ref. 14) we can see that for parameter regions where fixed points exist, the orientation of their manifolds is not suitable for homoclinic orbits of the type found in the previous section. However, observing the local phase portraits in the parameter region where there are no fixed points, the manifolds of the transversal periodic orbit γ are in a suitable position in order to produce *homoclinic tangencies* via the global reinjection mechanism.

To test this observation we used a multiple-shooting algorithm to locate the periodic orbit γ, together with its stable and unstable eigenvectors. We then shot a number of orbits forward in time starting a small distance of γ and on the unstable eigenvectors towards a Poincaré section, and similarly backwards in time on the stable eigenvector. By fixing η and adjusting β we were able to detect two homoclinic tangencies to γ (Fig. 8), labeled $t1$ and $t2$.

Figure 6 shows the numerical continuation of both homoclinic tangencies approaching the HSN singularity (see also the related Fig. 9). This result indicates that the limit

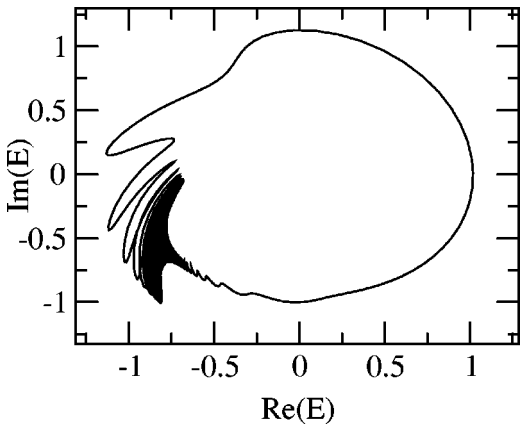

FIG. 8. The phase portrait of a homoclinic to the periodic orbit γ. γ lies within the densely oscillating region, $\theta=1.25$, $\eta=-0.32$, $\beta=0.1944960$.

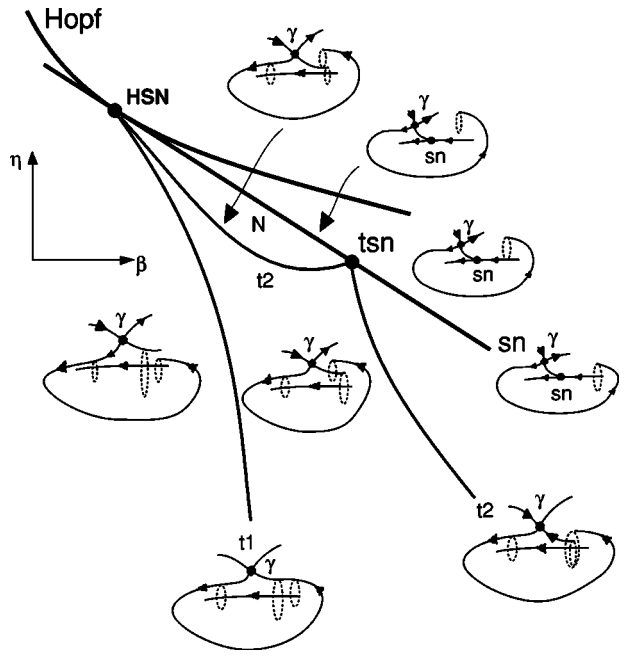

FIG. 9. Schematic bifurcation diagram η vs β. The two-dimensional manifolds of the periodic orbit γ are emphasized by the dotted curves. The HSN point, together with the saddle-node (sn) and Hopf bifurcation are shown. (tsn) corresponds to the creation of a heteroclinic cycle between the periodic orbit γ and the saddle-node fixed point.

point of these global bifurcations seems to be the HSN singularity. This can be understood by studying in more detail the boundary of the existence of γ together with its manifold orientation. On the one hand the locus of existence is bounded for small enough β by a saddle-node bifurcation [shown in Fig. 4(a)], and by the Hopf bifurcation to the right. We can even sharpen the boundary of existence by noting that at the saddle-node bifurcation of equilibriums, the stable manifold of γ ''merges'' with the 2-dimensional manifold of the saddle-node fixed point.[26] Also as the radius of γ decreases as one approaches the HSN point, one may expect that the homoclinic tangencies also approach the HSN point.

To illustrate in more detail how the tangencies behave as we approach the HSN point, we display in Fig. 10 three parameter cuts for fixed values of η, displaying the relative position of the invariant manifolds on a suitable Poincaré section as β is changed. We note that the chosen (local) Poincaré section $\Pi:\{x \in \mathrm{Re}(E)=0\}$ is not a ''standard'' section (i.e., the section does not intersect the periodic orbit) for studying homoclinics to periodic orbits. Nevertheless it is a section transversal to the flow in the region of interest which has the advantage of showing the closed topology these manifold have in our case. Notice that the intersection points of a stable and an unstable manifold correspond to intersection points in the typical Poincaré section $W=l$, for a suitable l where the periodic orbit and the stable and unstable manifold crosses Π. Whenever there is no l such that a manifolds crossing occurs, then the manifolds in Π' do not intersect.

The first row displays how the unstable manifold (inside) grows, becomes tangent and creates a pair of homoclinic orbits. This case corresponds to the tangency $t1$, and it behaves similarly for other constant η parameter cuts. The following rows illustrate how the $t2$ tangency may develop. Two cases are observed: (a) the stable manifold of γ shrinks to a point at the saddle-node bifurcation of equilibrium *outside* of the unstable manifold (second row), (b) it shrinks to a point *inside* the unstable manifold (last row). The third row shows approximately the transition point where the unstable manifold of γ just merges into the center manifold of the saddle-node equilibrium, producing a heteroclinic cycle $\Gamma_{\gamma\text{-SN}}$ between γ and the saddle-node fixed point. In Fig. 9 we display a schematic bifurcation diagram, displaying the position of the global invariant manifolds of the most relevant objects.

This new transition point corresponds to another codimension 2 global bifurcation. The relevance of it may be understood by studying a return map for both cases. For case (a) it is clear that any orbit leaving the unstable manifold of γ after one global excursion will never return to the neighborhood of the periodic orbit, for all the interval of parameter $\beta_{t2}<\beta<\beta_{\mathrm{SN}}$. On the other hand for case (b) we expect that further iterations of the return map may produce subsidiary homoclinic tangencies to γ (with $n>1$ global excursions).

To complete the picture we investigated the organization of the periodic orbits approaching the homoclinic tangencies. Figure 11 shows the period versus β continuation for a constant $\eta=-0.32$, starting from the orbit at $\beta=0$ and $(R,W)=(A^2,0)$, the unperturbed laser. It is observed that in contrast to the traditional Šil'nikov periodic orbit organization found for Type III (Fig. 5, Ref. 5), the periodic orbits became asymptotic to the values corresponding to the tangencies. Physically, as we increase β, these solutions corresponds to pulses which develop small oscillations in the amplitude of the electric field, and its phase is unbounded; asymptotically these small oscillations approach closer and closer the undamped relaxation oscillation γ (see Fig. 12).

The bifurcation scenario for homoclinic tangencies has been studied theoretically by Gaspard and Wang[27] where they report that two sequences of saddle-node bifurcations accumulate to the parameter values where each tangency occurs. More recently Hirshberg and Laing[28] developed a return map model close to a Takens–Bogdanov degenerate point where they observe that for high enough periods, *both* periodic orbits created at a saddle-node bifurcations die at another saddle-node bifurcation associated to the other tangency, forming ''bubbles'' or ''isola'' of periodic orbits in parameter space.

The family of periodic orbits in Fig. 11 seems to be bounded by the $t2$ tangency. However by the previous discussion on a return map, it allows the possibility of the existence of unstable orbits in the region between $t2$ tangency and the creation of the saddle-node bifurcation. For this we performed numerical integrations starting at the Poincaré section and inside the stable manifold. For negative time steps, in Fig. 13 we display the crossings with the Poincaré section, together with a phase-portrait. This shows the existence of a repeller inside the stable manifold of γ which turns into a periodic orbit of very high period as the stable manifold shrinks. At $\beta=0.1969<\beta_{\mathrm{SN}}$ we find the period of this unstable orbit $P\approx 2500$.

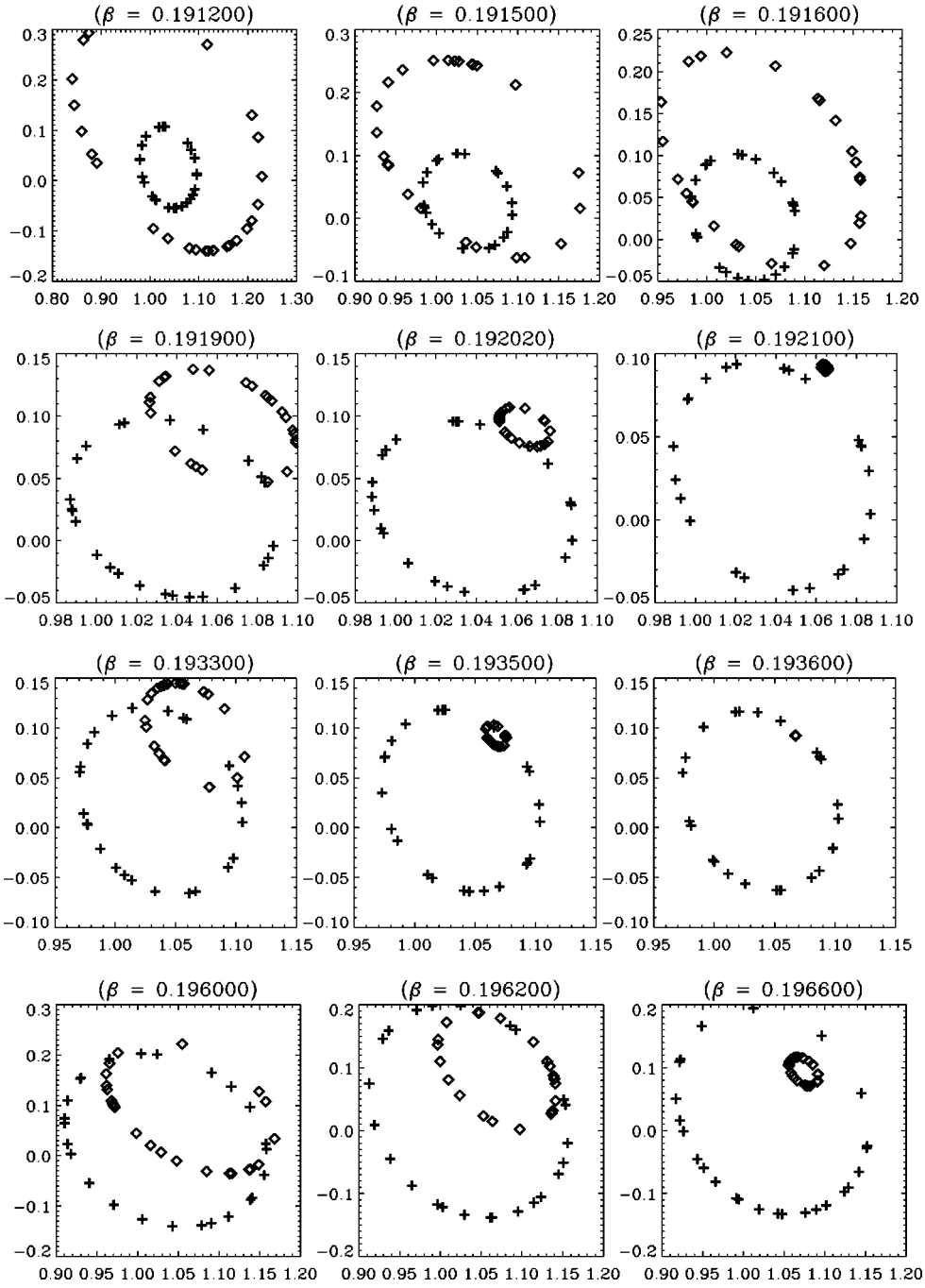

FIG. 10. Manifolds of periodic orbit γ on the Poincaré section $\mathrm{Re}(E)=0$. (From the top to the bottom) First row: crossing of tangency $t1$ at $\eta=-0.315$. Second row: crossing of tangency $t2$ at $\eta=-0.315$. Third row: crossing of tangency $t2$ at $\eta=-0.3175$. Fourth row: crossing of tangency $t2$ at $\eta=-0.323$, $(\theta=1.25)$. Crosses corresponds to the unstable manifold and diamonds to the stable manifold of γ. The coordinates of each panel correspond to $[\mathrm{Im}(E),W]$.

Finally, we note on passing that the analysis in Ref. 6 completes the study of the effects of the HSN bifurcation on LIS by describing the case of very low detuning (Type II of HSN).

V. DISCUSSION

We have shown that in the rate equations for a laser with injected signal, the detuning θ plays an important double role in determining the type of *local* bifurcations close to the locking regime, and changing the kind of *global* bifurcations.

We presented a systematic order-by-order analysis of the LIS equations starting with the Adler equation at lowest order, all the way up to the averaged model, accurate up to second order in the involved variables. Moreover, perturbation corrections beyond the averaged model give a sound basis to the geometrical model of LIS proposed in Ref. 5.

We analyzed with normal form theory how the Type of the Hopf-saddle-node bifurcation changes with the parameters, verifying that the classification (1) found by Solari and Oppo[2] in an averaged system is accurate.

This change of type as θ is varied should affect the global bifurcations involving the invariant sets of the HSN bifurcation. We therefore extended our previous numerical findings[5] showing that for $\theta>\theta_{\text{I-III}}\approx\sqrt{3}+\mathcal{O}(\cdot)$ the main scenario for the development of ''chaos'' comes from the Šil'nikov phenomenon[14,15] (homoclinic bifurcation to a saddle-focus fixed point) interacting with a saddle-node bifurcation. A new scenario was found in the region $\theta<\theta_{\text{I-III}}$

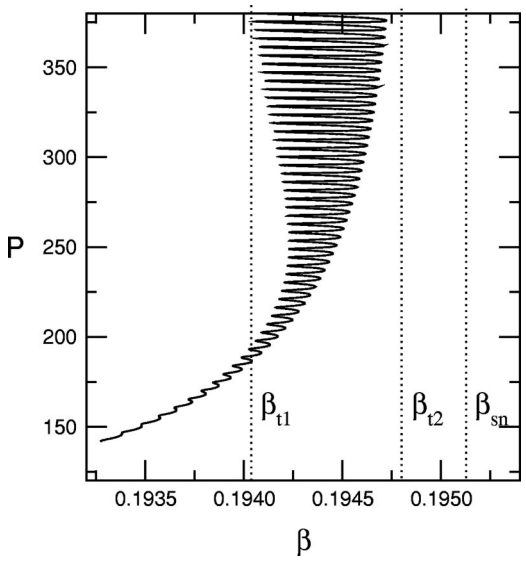

FIG. 11. Period (P) vs β bifurcation diagram for periodic orbits ($\theta=1.25$, $\eta=-0.32$). The homoclinic tangencies occur at $\beta_{t1}=0.1940533$ and $\beta_{t2}=0.1947231$. The vertical dashed lines mark the occurrence of the homoclinic tangencies $t1$ ($\beta_{t1}=0.1940533$), $t2$ ($\beta_{t2}=0.1947231$), and the saddle-node bifurcation of fixed points (sn).

$\approx\sqrt{3}+\mathcal{O}(\cdot)$, where homoclinic tangencies to a periodic orbit were found to originate from the HSN bifurcation. Both the saddle-fixed points and the periodic orbit belong to the unfolding of the Hopf-saddle-node local bifurcation.

The above results point to the conjecture that there is a codimension-3 global bifurcation involving the Hopf-saddle-node local singularity and the global reinjection present in this laser in a wide range of parameters (at least $\theta_{\text{II-I}}<\theta<\theta_{\text{I-III}}<2.0$). We hope these numerical findings will open the way to new theoretical models to understand more closely the unfolding of this degenerate bifurcation.

Most important for the physicists is that the region of existence of the Šil'nikov phenomenon is bounded for low enough injection amplitude β by the disappearance of the locking states, while for the homoclinic tangencies the chaotic regime occurs for injection amplitudes β *just* "before" the locking states appear.

As it is well known, estimation of θ in real experiments is difficult. We thus hope that with a close study of the existence of locking states and chaotic regimes it might be possible to determine in which type the laser is working, and contrast our numerical predictions.

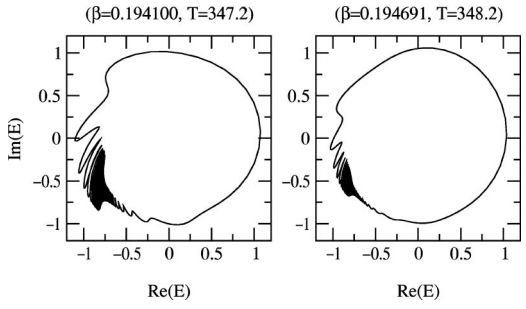

FIG. 12. Phase portraits for two saddle orbits close to tangency $t1$ (left) and $t2$ (right). T corresponds to the period of the orbit ($\eta=-0.32,\theta=1.25$).

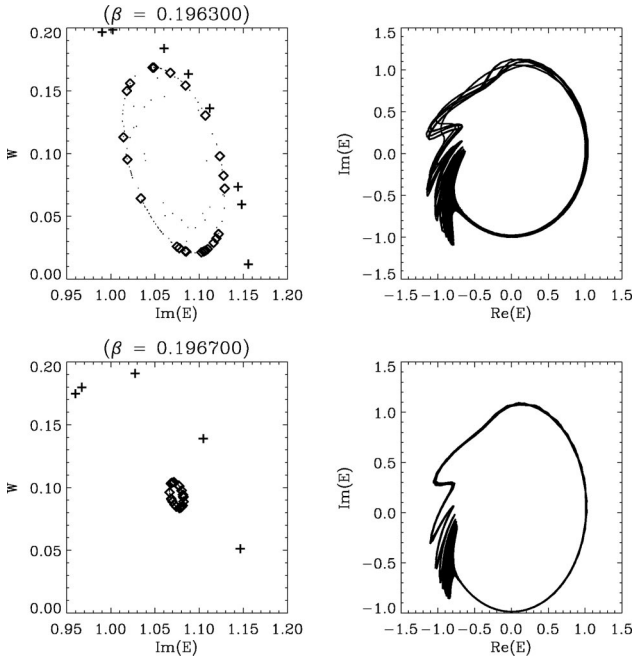

FIG. 13. The left panel shows the Poincaré sections as in Fig. 10, while the right panel shows the corresponding phase-portrait of unstable orbits. Notice that as β increases the periodic orbit diverges in period ($\eta=-0.323,\theta=1.25$).

ACKNOWLEDGMENTS

H.G.S. and M.A.N. acknowledge the support of the Fundación Antorchas and STINT and M.G.Z. acknowledges support from FOMEC-UBA. This work was partially financed by the University of Buenos Aires under Grant No. TW04.

APPENDIX A: THE AVERAGING PROCEDURE IN REF. 3

We will now apply the averaging procedure to the relaxation oscillations motion of the laser with injected signal model as written in Eq. (1) of Ref. 4,

$$\dot{E}=\frac{\xi}{2}(1+i\alpha)nE+\kappa_{\text{inj}}E_{\text{inj}}e^{i\omega_{\text{inj}}t},$$
$$\dot{n}=-2\lambda_R n-(\Gamma_0+\xi n)(|E|^2-P_0), \tag{A1}$$

with the electric field E, inversion population n, linewidth enhancement factor α, injection rate κ_{inj}, detuning ω_{inj}.

We first re-write the system in a more convenient way, following as close as possible the transformations used in Ref. 3: $E(t)\to E(t)/\sqrt{P_0}\,e^{-i\omega_{\text{inj}}t}$, and rescaled $n\to(\xi/\omega_R)\,n$, $t=(\tau/\omega_R)$, with $\omega_R=\sqrt{\xi\Gamma_0P_0}$, we arrive at the system

$$E'=\frac{1+i\alpha}{2}nE-i\eta E+\kappa,$$
$$n'=1-\chi n(1+g|E|^2)-|E|^2 \tag{A2}$$

where $'=\mathrm{d}/\mathrm{d}\tau$ and

$$\eta=\frac{\omega_{\rm inj}}{\omega_R},\quad \chi=\frac{2\lambda_R-\xi P_0}{\omega_R},\quad g\chi=\frac{\xi P_0}{\omega_R},\quad \kappa=\frac{\kappa_{\rm inj}E_{\rm inj}}{\omega_R\sqrt{P_0}}. \tag{A3}$$

Next we write the complex variable E in polar coordinates (v,ψ) by $E=e^{v/2-i(\psi-\alpha v/2+\alpha_1)}$, where α_1 is a constant to be determined at the end. Expanding in powers of v we obtain

$$\begin{aligned} v' &= n-\kappa F(v,n,\psi),\\ n' &= -v-\frac{v^2}{2}+O(v^3)+\chi G(v,n,\psi),\\ \psi' &= \eta+\kappa H(v,n,\psi). \end{aligned} \tag{A4}$$

To apply the averaging theorem we must change (A4) to a ''slow'' system, which would require to find an analytic solution to the nonharmonic oscillator $v''+v+v^2/2=0$.

The procedure in Ref. 3 considers instead only the order $O(v)$ in the equation and therefore studies the resulting system as a perturbation of the harmonic oscillator $v''+v=0$. This will of course imply that the correct solution is valid *up to first order* yielding accordingly inaccurate results for second order and higher. For the sake of comparison of the final averaged equations we apply the averaging operator also over the $O(v^2,v^3)$ terms. Following the variables defined in Ref. 3,

$$v=\frac{2\rho}{\sqrt{1+\alpha^2}}\sin(-t+\zeta),\quad n=\frac{2\rho}{\sqrt{1+\alpha^2}}\cos(-t+\zeta), \tag{A5}$$

and averaging over one RO period,[29] we obtain Eq. (3) in Ref. 4,

$$\begin{aligned} \dot\rho &= -\left(\Gamma-\frac{K}{2}\sin(\phi+\alpha)\right)\\ &\quad\times\rho-\left(\frac{B}{2(1+\alpha^2)}-\frac{K}{16}\sin(\phi+2\alpha)\right)\rho^3,\\ \dot\phi &= \omega-K\cos\phi-\frac{K}{4}\cos(\phi+\alpha)\rho^2, \end{aligned} \tag{A6}$$

choosing $\alpha_1=A_\alpha/2+\pi/2$, $A_\alpha=2\arctan(\alpha)$ and

$$\begin{aligned} \Gamma &= \frac{\chi}{2}(1+g)=\frac{\lambda_R}{\omega_R},\\ K &= \frac{\kappa}{\cos(\alpha/2)}=\frac{k_{\rm inj}E_{\rm inj}}{\omega_R\sqrt{P_0}}\sqrt{1+\alpha^2},\quad B=\frac{\omega_R}{2\Gamma_0}. \end{aligned} \tag{A7}$$

This corresponds with the parameter identification published in Ref. 4 [except that we did not include for simplicity that (A5) depends on the rescaled relaxation oscillation frequency $\Omega(\bar n)$].

We have thus recovered the averaged equation studied in Ref. 4 by the standard averaging method, which indirectly shows the procedure used in Ref. 3 is correct *only up to first order in* ρ. The second order terms are important for determining the change of signs in the coefficients of the HSN normal form, and consequently inaccuracies in the second order terms will be reflected when studying the normal form. This explains why the (otherwise thorough) normal form analysis carried out in Ref. 4 only reveals Type II for $0<\theta<1$ and Type III for $1<\theta$. This was recognized as an anomalous transition since it requires at a single critical parameter ($\theta=1$) two normal form coefficients to disappear simultaneously. The order-consistent results of Ref. 2 revisited in this manuscript include the intermediate Type I regime and provides a smooth transition between types, involving for each critical parameter only a single zero nonlinear term. Also, a more careful analysis of the third order terms in ρ in the normal form is required to study the stability of the tori as intended in Ref. 4.

APPENDIX B: DERIVATION OF NORMAL FORM COEFFICIENTS

We will now give the derivation of the nonlinear coefficients of the Hopf-saddle-node normal form in terms of derivatives of the linearized vector field. This derivation follows closely the analogous derivation for the Hopf bifurcation in Ref. 14 (p. 163). First we write in complex variables the HSN normal form at the singularity (26) ($\mu=\nu=0$) using $w=re^{i\zeta}$,

$$w'=i\omega+(a+id)wz+\mathcal{O}(3),\quad z'=bw\bar w+cz^2+\mathcal{O}(3), \tag{B1}$$

with a, b, c, d real coefficients, and the linearized equations (28) around the origin using $\xi=x+iy$,

$$\begin{aligned} \xi' &= i\omega+f(\xi,\bar\xi,v),\\ v' &= h(\xi,\bar\xi,v), \end{aligned} \tag{B2}$$

with $f(\xi,\bar\xi,v)=(F+iG)[(\xi+\bar\xi)/2,(\xi-\bar\xi)/2i,v]$ a complex function, while $h(\xi,\bar\xi,v)=H[(\xi+\bar\xi)/2,(\xi-\bar\xi)/2i,v]$ is a real function. The overbar denotes a complex conjugation.

As we are interested in eliminating from (B2) as many second-order terms as possible, we expand f,h in power series as $f(w+\psi,\bar w+\bar\psi,z+\phi)=f_{\xi\xi}w^2/2+f_{\xi\bar\xi}w\bar w+f_{\bar\xi\bar\xi}\bar w^2/2+f_{\xi z}wz+f_{\bar\xi z}\bar wz+f_{zz}z^2/2+\mathcal{O}(3)$, where the subscript indexes stand for partial derivative, and propose a near-identity change of coordinates,

$$\xi=w+\psi(w,\bar w,z),\quad v=z+\phi(w,\bar w,z) \tag{B3}$$

where ψ and ϕ have only second-order monomials:

$$\begin{aligned} \psi(w,\bar w,z) &= A_1w^2+A_2w\bar w+A_3\bar w^2+A_4wz+A_5\bar wz\\ &\quad+A_6z^2+\mathcal{O}(3),\\ \phi(w,\bar w,z) &= B_1w^2+B_2w\bar w+B_3\bar w^2+B_4wz+B_5\bar wz\\ &\quad+B_6z^2+\mathcal{O}(3). \end{aligned}$$

Performing the change of coordinates, one arrives at a new vector field in terms of (w,z) where the second-order terms depend on the unknown constants (A_i,B_i). Comparing term by term to (B1) we are able to solve for all unknown coefficients in terms of derivatives of f and h (using $\omega\neq0$) except for

$$wz{:}\,a+id=f_{\xi z},\quad w\bar w{:}\,b=h_{\bar\xi\bar\xi},\quad z^2{:}\,c=h_{zz}/2. \tag{B4}$$

Note that these are exactly the resonant terms of the normal form of HSN, thus a (normal form) change of coordinates will never be able to eliminate them. Now returning to $x=(\xi+\bar{\xi})/2$ and $y=(\xi-\bar{\xi})/(2i)$ we have that $f_u=-(f_x-if_y)/2$, so we arrive to

$$a=\mathrm{Re}\, f_{\xi z}=(F_{xv}+G_{yv})/2,\quad b=h_{\xi\bar{\xi}}=(H_{xx}+H_{yy})/4,$$
$$d=\mathrm{Im}\, f_{\xi z}=(G_{xv}-F_{yv})/2,\quad c=h_{zz}/2=H_{vv}/2. \tag{B5}$$

For the interested reader who might want to compute the third-order terms of the HSN normal form, we refer to Ref. 30.

[1] R. Adler, Proc. IRE **34**, 351 (1946), reprinted in Proc. IEEE **61**, 1380 (1973).
[2] H. G. Solari and G.-L. Oppo, Opt. Commun. **111**, 173 (1994).
[3] P. C. D. Jagher, W. A. van der Graaf, and D. Lenstra, Quantum Semiclassic. Opt. **8**, 805 (1996).
[4] B. Krauskopf, W. A. van der Graaf, and D. Lenstra, Quantum Semiclassic. Opt. **9**, 797 (1997).
[5] M. G. Zimmermann, M. A. Natiello, and H. G. Solari, Physica D **109**, 293 (1997).
[6] C. Mayol, M. A. Natiello, and M. G. Zimmermann, Int. J. Bifur. Chaos (in press).
[7] J. R. Tredicce, F. T. Arecchi, G.-L. Lippi, and G. P. Puccioni, J. Opt. Soc. Am. B **2**, 173 (1985).
[8] Y. Kuznetsov, *Elements of Applied Bifurcation Theory*, No. 112 in Applied Mathematical Sciences (Springer-Verlag, Berlin, 1997).
[9] G.-L. Oppo, A. Politi, G.-L. Lippi, and F. T. Arecchi, Phys. Rev. A **34**, 4000 (1986).
[10] H. Zeglache and V. Zehblè, Phys. Rev. A **46**, 6015 (1992).
[11] L. A. Lugiato, L. M. Narducci, D. K. Bandy, and C. A. Pennise, Opt. Commun. **46**, 64 (1983).
[12] A. Politi, G. Oppo, and R. Badii, Phys. Rev. A **33**, 4055 (1986).
[13] P. A. Braza and T. Erneux, Phys. Rev. A **40**, 2539 (1989).
[14] J. Guckenheimer and P. J. Holmes, *Nonlinear Oscillations, Dynamical Systems and Bifurcations of Vector Fields* (Springer-Verlag, New York, 1983).
[15] S. Wiggins, *Introduction to Applied Nonlinear Dynamical Systems and Chaos*, No. 2 in Text in Applied Mathematics (Springer-Verlag, Berlin, 1991).
[16] L. P. Šil'nikov, Sov. Math. Dokl. **7**, 155 (1966).
[17] M. K. S. Yeung and S. Strogatz, Phys. Rev. E **58**, 4421 (1998); see erratum *ibid.* **61**, 2154 (2000).
[18] H. G. Solari, M. Natiello, and B. G. Mindlin, *Nonlinear Dynamics: A Two-Way Trip From Physics to Math* (Institute of Physics, Bristol, 1996).
[19] β will appear below as $\kappa=\beta/A$.
[20] In terms of the original variables (E,W), the rotational symmetry reads as $(E,W)\to(E\exp(i\psi_0),W)$ for arbitrary ψ_0 and the reflection symmetry reads as $(E,W)\to(E^*|E|^{i2\theta},W)$.
[21] G.-L. Oppo and A. Politi, Z. Phys. B: Condens. Matter **59**, 111 (1985).
[22] Whenever fixed points arise in a saddle-node bifurcation, it is expected that a ''local'' heteroclinic connection between both fixed points will exist for a small region where $\kappa>\kappa_{\mathrm{SN}}$. However, a ''global'' connection between the fixed points [as displayed in (10) for $r=0$] need not exist in general.
[23] E. Doedel and J. Kernévez, AUTO: *Software for Continuation Problems in Ordinary Differential Equations With Applications*, Tech. Rep., Applied Mathematics, California Institute of Technology, 1986.
[24] The transversal torus is destroyed in the homoclinic to the transversal orbit of the TB point.
[25] B. Deng, Trans. Am. Math. Soc. **331**, 15 (1992).
[26] This holds for parameter values sufficiently close to the HSN, otherwise one expects an open region of parameters where the intersection of these 2-dimensional manifolds occurs.
[27] P. Gaspard and X.-J. Wang, J. Stat. Phys. **48**, 151 (1987).
[28] P. Hirschberg and C. Laing, Physica D **89**, 1 (1995).
[29] Note that in Ref. 2 a different choice of polar coordinates (r,ψ) has been chosen, thus changing the A_α and α_1. Also in Ref. 2 there is a typo in the averaged equations (3.4), $\dot{r}=-(r/2)(\cdots)$.
[30] R. W. Wittenberg and P. Holmes, Physica D **100**, 1 (1997).